

Electronic structure of $\text{La}_{1.85}\text{Sr}_{0.15}\text{CuO}_4$: Characterization of a Fermi-level band crossing

Jason K. Perry and Jamil Tahir-Kheli

First Principles Research, Inc., 8391 Beverly Boulevard, Suite No. 171, Los Angeles, California 90048

(Received 8 September 1997; revised manuscript received 12 June 1998)

We present the results of a Hubbard model for optimally doped $\text{La}_{2-x}\text{Sr}_x\text{CuO}_4$. This model uses parameters derived from Becke-Lee-Yang-Parr calculations on the cluster CuO_6 . It explicitly includes the Cu $d_{x^2-y^2}$ and d_{z^2} orbitals, the O p_σ orbitals, and the apical O p_z orbitals. We find that when the mean-field equation is appropriately modified to include a self-interaction correction, a crossing of two bands is observed in the vicinity of the Fermi level for the optimally doped superconductor. This crossing rigorously occurs along the $(0,0) - (\pi/a, \pi/a)$ direction of the two-dimensional (2D) Brillouin zone. The crossing arises due to the overlap of a broad “ B_{1g} ” band dominated by Cu $d_{x^2-y^2}$ character and a narrower “ A_{1g} ” band dominated by Cu d_{z^2} character. We conclude that optimal doping of $\text{La}_{2-x}\text{Sr}_x\text{CuO}_4$ and related materials is achieved when the Fermi level coincides with this crossing. At this point, formation of Cooper pairs between the two bands (i.e., interband pairing or IBP) leads to superconductivity. We further extend our conclusions to $\text{YBa}_2\text{Cu}_3\text{O}_{6+\delta}$ and offer a simple explanation for the seemingly complex behavior of T_c as a function of doping in this material. This behavior can be understood on the basis of multiple band crossings predicted from geometric considerations. [S0163-1829(98)04242-8]

I. INTRODUCTION

Eleven years have elapsed since the discovery of high-temperature copper oxide superconductors,¹ yet there is still no consensus on the physics of the pairing mechanism. In this work, we focus on the recent suggestion by Tahir-Kheli² that superconductivity arises in these materials due to interband pairing (IBP). That is, Cooper pairing of electrons belonging to two distinct bands may be the cause of superconductivity. Such a proposal is appealing as it readily explains why superconductivity is only observed at very specific doping levels. $\text{La}_{2-x}\text{Sr}_x\text{CuO}_4$, for instance, shows an optimal T_c of 39 K when $x=0.15$, but superconductivity quickly vanishes as the doping level is changed.³ The IBP theory only requires that two bands cross. Should such a crossing exist, then optimal doping is achieved when the Fermi level coincides with this crossing. Precise doping levels are needed for this to occur.

In this work, we argue that no such band crossings have been observed for these materials using conventional local-density approximation (LDA) band-structure calculations due to a breakdown in the mean-field equation. As has been stressed by Svane⁴ and others⁵ in the limit of weakly interacting particles a self-interaction correction to the mean-field equation becomes necessary. Such a correction has been applied in a limited way to describe the antiferromagnetic state of undoped La_2CuO_4 . Here we suggest that the self-interaction correction is equally important to the metallic phase of the doped material and find that its general inclusion in a simple Hubbard model leads to a dramatically different band structure with the critical feature of a Fermi-level band crossing. The crossing is calculated to occur just 0.15 eV below the Fermi level for the optimally doped material between one band which is dominated by Cu $d_{x^2-y^2}$ character and a second which is dominated by Cu d_{z^2} character. Moreover, we find that when the model is empirically adjusted to include missing electronic effects, the crossing can

be seen to occur at exactly the Fermi level. As detailed in the accompanying article by Tahir-Kheli,⁶ a number of key experimental observations that are otherwise anomalous, such as the temperature dependence of the NMR spin-relaxation rates and Knight shifts, the Hall effect, the resistivity, and Josephson tunneling, are easily explained with the resulting band structure and the IBP model.

What follows is a detailed account of how this Hubbard model was developed for $\text{La}_{1.85}\text{Sr}_{0.15}\text{CuO}_4$. The resulting band structure is discussed at length. In addition we speculate that other copper oxide superconducting materials can be understood based largely on geometric constraints. As an example, we suggest simple arguments as to why $\text{YBa}_2\text{Cu}_3\text{O}_{6+\delta}$ appears to show two characteristic T_c 's over an extended doping range.

II. CALCULATIONAL DETAILS

A. Cluster calculations

Parameters for the Hubbard model were extracted from restricted open-shell density-functional (DFT) calculations on the cluster CuO_6 . These calculations used the gradient-corrected Becke-Lee-Yang-Parr (BLYP) functional⁷ with the standard $6-31+G^*$ basis set⁸ on the oxygen atoms and Hay and Wadt's⁹ effective core potential and basis set on the copper. All calculations were performed using the JAGUAR (Ref. 10) *ab initio* electronic structure program on a dual processor 200 MHz Pentium Pro running Linux.

The CuO_6 cluster was embedded in a point-charge array of 1364 ions. The ions had the formal charges of +2.000 for Cu, -1.925 for O, -2.000 for apical O, and +2.925 for La/Sr. The total cluster and point-charge array had the D_{4h} symmetry of the tetragonal unit cell and was five unit cells wide (18.940 Å) in the a and b directions and three unit cells tall (39.618 Å) in the c direction. Fractional charges were used at the edges. It should be noted that at the low tempera-

TABLE I. Crystal structure of $\text{La}_{1.85}\text{Sr}_{0.15}\text{CuO}_4$ (in Å).

a	3.788
b	3.788
c	13.206
Cu	(0.000,0.000,0.000)
O(1)	(0.500,0.000,0.000)
O(2)	(0.000,0.000,0.182)
La/Sr	(0.000,0.000,0.361)

tures where superconductivity appears, the crystal shows a C_{2h} distortion to an orthorhombic unit cell. This should be a relatively small perturbation, so for the sake of simplicity the higher symmetry structure was used. However, we note here that the distortion will have some important implications in regard to superconductivity. This will be discussed below. The tetragonal crystal structure was taken from Hazen¹¹ and is given in Table I and shown in Fig. 1.

To obtain the Hubbard parameters, the density of a single state was optimized and the resulting orbitals were localized. By then making specific combinations of the localized orbitals and not allowing them to relax in subsequent DFT calculations, it was then possible to determine the Hubbard parameters associated with the localized orbitals. For example, evaluating the energy of the state where there is one hole in the localized Cu $d_{x^2-y^2}$ orbital (${}^2B_{1g}[\text{CuO}_6]^{-10}$) and using the state where there are no holes at all (${}^1A_{1g}[\text{CuO}_6]^{-11}$) as a reference yields the orbital energy for Cu $d_{x^2-y^2}$. Evaluating the energy of the state where there are two holes in the Cu $d_{x^2-y^2}$ orbital (${}^1A_{1g}[\text{CuO}_6]^{-9}$) then leads to the self-Coulomb term for this orbital. Similarly, evaluating the energy of a state where there is one hole in the plus combination of the localized Cu $d_{x^2-y^2}$ and O p_σ orbitals as compared to the state where there is one hole in the minus combination of these orbitals leads to the matrix element coupling the two orbitals. Clearly, all principle nearest-neighbor Hubbard parameters describing the set of Cu, O, and apical O orbitals can be obtained in such a fashion using just this single CuO_6 cluster.

The density was optimized for the undoped ground state, ${}^2B_{1g}[\text{CuO}_6]^{-10}$. This state has one hole in an orbital that is about 50% Cu $d_{x^2-y^2}$ and 50% O p_σ . The state was chosen because it represents the closest approximation to the true density that can be obtained with this finite cluster. Note however that the point-charge array reflects a doped state ($x=0.15$) so the total charge on the system (cluster+point charges) is -0.3 . While it was not possible to treat the cluster with a fractional charge to make the total charge on the system neutral, this discrepancy was effectively removed by the procedure described below in Sec. II B.

The orbitals were localized using the Pipek-Mezey¹² localization procedure which maximizes the sum of the squares of the atomic Mulliken populations over basis functions. This procedure was done in several steps. First, orbitals within a given irreducible representation were localized and identified. This produced localized Cu $d_{x^2-y^2}$ (B_{1g}) and d_{z^2} (A_{1g}) orbitals, and symmetry combinations of the O p_σ (A_{1g} , E_u , and B_{1g}), O p_π (B_{2g} , E_u , and A_{2g}), and apical O p_z (A_{1g} and A_{2u}) orbitals. The procedure was then used on

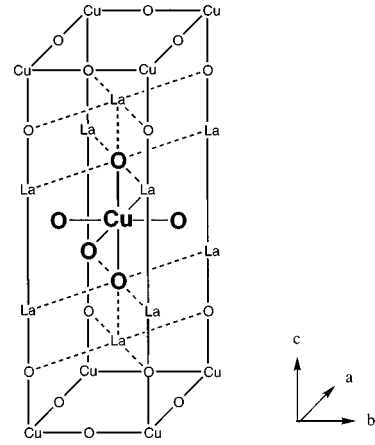


FIG. 1. Tetragonal unit cell of $\text{La}_{1.85}\text{Sr}_{0.15}\text{CuO}_4$ showing the CuO_6 cluster used in the DFT calculations in bold.

the symmetry combinations of the oxygen orbitals to obtain completely localized O p_σ , O p_π , and apical O p_z orbitals.

Hubbard parameters were derived by evaluating the DFT energies with fixed orbitals (i.e., non-self-consistent field) as follows:

- (1) The energy of the ${}^1A_{1g}[\text{CuO}_6]^{-11}$ state (having no holes) was evaluated. This was used as our reference state.
- (2) The energies of the doublet $[\text{CuO}_6]^{-10}$ states (each having a single hole in one of the localized orbitals) were evaluated. This yielded the orbital energies, E_i^0 .
- (3) The energies of the singlet $[\text{CuO}_6]^{-9}$ states (each having two holes in one of the localized orbitals) were evaluated. This yielded the self-Coulomb repulsion energies, J_{ii} .
- (4) The Hartree-Fock energies of the triplet and open-shell singlet $[\text{CuO}_6]^{-9}$ states (each having two holes in different localized orbitals) were evaluated. This yielded the exact exchange energy between orbitals, K_{ij} .
- (5) The energies of the triplet $[\text{CuO}_6]^{-9}$ states (each having two holes in different localized orbitals) were evaluated. This yielded the Coulomb repulsion energy between orbitals, J_{ij} .
- (6) The energies of the doublet $[\text{CuO}_6]^{-10}$ states (each having one hole in either the plus or minus combination of pairs of localized orbitals) were evaluated. This yielded the matrix elements coupling pairs of orbitals, T_{ij} . Note that the fully symmetric combinations of the oxygen orbitals were used in the evaluation of these terms rather than the completely localized orbitals.

Parameters obtained from this procedure are listed in Table II. This parameter set will be referred to as the unscaled set.

Perhaps the main limitation in the method used here to obtain the Hubbard parameters is that the orbitals were not allowed to relax for different states. This results in Coulomb interactions which are too high and orbital energies which are too low. To determine the effect that orbital relaxation has on our Hubbard parameters, we looked at isolated Cu, O, and apical O atoms in the full point-charge array. We derived orbital energies and Coulomb interactions for these lone atoms using both fixed orbitals and fully optimized orbitals.

TABLE II. Unscaled Hubbard parameters (in eV). E is an orbital energy, T is an orbital coupling matrix element, J is a Coulomb repulsion term, and K is an exchange energy term.

$E(x^2-y^2)$	-3.109	$J(x^2-y^2/z^2)$	25.563	$K(x^2-y^2/z^2)$	1.219
$E(z^2)$	-3.338	$J(x^2-y^2/O p_\sigma)$	7.999	$K(x^2-y^2/O p_\sigma)$	0.081
$E(O p_\sigma)$	-10.417	$J[x^2-y^2/O(2)p_z]$	6.471	$K[x^2-y^2/O(2)p_z]$	0.028
$E[O(2)p_z]$	-12.442	$J(x^2-y^2/O p_\pi)$	7.053	$K(x^2-y^2/O p_\pi)$	0.006
$J(x^2-y^2/x^2-y^2)$	29.281	$J(z^2/O p_\sigma)$	6.471	$K(z^2/O p_\sigma)$	0.028
$J(z^2/z^2)$	25.990	$J[z^2/O(2)p_z]$	6.855	$K[z^2/O(2)p_z]$	0.262
$J(O p_\sigma/O p_\sigma)$	17.375	$J(z^2/O p_\pi)$	6.813	$K(z^2/O p_\pi)$	0.008
$J[O(2)p_z/O(2)p_z]$	11.365	$J(O p_\sigma/O p'_\sigma)$	5.345	$K(O p_\sigma/O p'_\sigma)$	0.035
$T(x^2-y^2/O p_\sigma)$	1.347	$J(O p_\sigma/O p''_\sigma)$	3.890	$K(O p_\sigma/O p''_\sigma)$	0.008
$T(z^2/O p_\sigma)$	0.514	$J[O p_\sigma/O(2)p_z]$	5.144	$K[O p_\sigma/O(2)p_z]$	0.211
$T[z^2/O(2)p_z]$	1.076	$J(O p_\sigma/O p_\pi)$	14.299	$K(O p_\sigma/O p_\pi)$	0.677
$T(O p_\sigma/O p'_\sigma)$	0.368	$J(O p_\sigma/O p'_\pi)$	5.548	$K(O p_\sigma/O p'_\pi)$	0.092
$T(O p_\sigma/O p''_\sigma)$	-0.041	$J(O p_\sigma/O p''_\pi)$	3.953	$K(O p_\sigma/O p''_\pi)$	0.008
$T[O p_\sigma/O(2)p_z]$	0.078	$J[O(2)p_z/O(2)p'_z]$	3.502	$K[O(2)p_z/O(2)p'_z]$	0.098
$T[O(2)p_z/O(2)p'_z]$	0.493	$J[O(2)p_z/O p_\pi]$	4.868	$K[O(2)p_z/O p_\pi]$	0.087

The Coulomb energies were found to uniformly scale as 0.7 when relaxation was introduced. The orbital energies (defined here as $E(\phi^2) - E(\phi) - J_{jj}$) did not scale quite as uniformly, so different scales were used for Cu, O, and apical O. We found that the orbital energy for Cu scaled as 0.6, for O as 0.8, and for apical O as 0.7. We applied all these scales to the Hubbard parameters listed in Table II to produce the set listed in Table III. It is this corrected set that was used in our final calculations. We should point out that we experimented with some other scaled sets (such as that obtained from uniformly scaling both the orbital energies and Coulomb terms by 0.7) and found no qualitative changes in the band structure. Even when the unscaled set was used, the same basic features were still observed.

The Hubbard model that was developed included explicitly the Cu $d_{x^2-y^2}$ and d_{z^2} orbitals, the O p_σ orbitals (two per unit cell), and the apical O p_z orbitals (two per unit cell). This led to a total of six bands. Solving the Hubbard model was done in two parts. The first took the input parameters (orbital energies and coupling terms) and found the single

electron energies $\epsilon_n(k)$ and wave functions $\phi_n(k)$ where n is the band index. These k states were filled to the required doping level and the orbital occupations were evaluated. In the second step, these orbital occupations were used to re-evaluate the orbital energies. The procedure was repeated until self-consistency was achieved. The Hubbard model is explained in more detail in the preceding paper.⁶

The Hubbard model was solved assuming no dispersion in the z direction. In calculating the density of states, however, z -axis dispersion was included perturbatively by assuming a dominant coupling through the apical O p_z orbitals.

B. Orbital energy evaluation

When orbital occupations were evaluated in the diagonalization step, the change in the Coulomb field had to be incorporated into the orbital energies, E_i . This was done by dividing up this field into that due to the CuO_6 cluster and that due to the point-charge array. Since the reference orbital energies, E_i^0 , were originally defined for the case in which

TABLE III. Scaled Hubbard parameters (in eV). E is an orbital energy, T is an orbital coupling matrix element, J is a Coulomb repulsion term, and K is an exchange energy term.

$E(x^2-y^2)$	1.063	$J(x^2-y^2/z^2)$	17.894	$K(x^2-y^2/z^2)$	1.219
$E(z^2)$	0.596	$J(x^2-y^2/O p_\sigma)$	5.599	$K(x^2-y^2/O p_\sigma)$	0.081
$E(O p_\sigma)$	-10.071	$J[x^2-y^2/O(2)p_z]$	4.532	$K[x^2-y^2/O(2)p_z]$	0.028
$E[O(2)p_z]$	-8.709	$J(x^2-y^2/O p_\pi)$	4.937	$K(x^2-y^2/O p_\pi)$	0.006
$J(x^2-y^2/x^2-y^2)$	20.497	$J(z^2/O p_\sigma)$	5.318	$K(z^2/O p_\sigma)$	0.028
$J(z^2/z^2)$	18.193	$J[z^2/O(2)p_z]$	4.799	$K[z^2/O(2)p_z]$	0.262
$J(O p_\sigma/O p_\sigma)$	12.163	$J(z^2/O p_\pi)$	4.769	$K(z^2/O p_\pi)$	0.008
$J[O(2)p_z/O(2)p_z]$	7.956	$J(O p_\sigma/O p'_\sigma)$	3.742	$K(O p_\sigma/O p'_\sigma)$	0.035
$T(x^2-y^2/O p_\sigma)$	1.347	$J(O p_\sigma/O p''_\sigma)$	3.601	$K(O p_\sigma/O p''_\sigma)$	0.008
$T(z^2/O p_\sigma)$	0.514	$J[O p_\sigma/O(2)p_z]$	3.601	$K[O p_\sigma/O(2)p_z]$	0.211
$T[z^2/O(2)p_z]$	1.076	$J(O p_\sigma/O p_\pi)$	10.009	$K(O p_\sigma/O p_\pi)$	0.677
$T(O p_\sigma/O p'_\sigma)$	0.368	$J(O p_\sigma/O p'_\pi)$	3.884	$K(O p_\sigma/O p'_\pi)$	0.092
$T(O p_\sigma/O p''_\sigma)$	-0.041	$J(O p_\sigma/O p''_\pi)$	2.767	$K(O p_\sigma/O p''_\pi)$	0.008
$T[O p_\sigma/O(2)p_z]$	0.078	$J[O(2)p_z/O(2)p'_z]$	2.451	$K[O(2)p_z/O(2)p'_z]$	0.098
$T[O(2)p_z/O(2)p'_z]$	0.493	$J[O(2)p_z/O p_\pi]$	3.408	$K[O(2)p_z/O p_\pi]$	0.087

all CuO_6 orbitals were doubly occupied (${}^1A_{1g}[\text{CuO}_6]^{-11}$), the change in the orbital energies (E_i) due to the change in the occupation of the CuO_6 orbitals (N_i) were determined from

$$E_i = E_i^0 - (2 - N_i)J_{ii} - \sum_{j \neq i} (2 - N_j) \left(J_{ij} - \frac{1}{2} K_{ij} \right), \quad N_i > 1 \quad (1)$$

$$E_i = E_i^0 - J_{ii} - \sum_{j \neq i} (2 - N_j) \left(J_{ij} - \frac{1}{2} K_{ij} \right), \quad N_i \leq 1 \quad (2)$$

where the Cu $d_{x^2-y^2}$ and d_{z^2} orbitals, the four O p_σ orbitals and the two apical O p_z orbitals of the CuO_6 cluster were included in the summation.

The Coulomb potential due to the changing long-range field was evaluated by first subtracting off the potential due to the 1364 ion point-charge array used in the DFT calculations. This was evaluated as a classical point-charge Coulomb interaction at each of the Cu, O, and apical O sites of the CuO_6 cluster. A similar Coulomb interaction was evaluated with a larger array having 22 374 ions [17 unit cells wide in the a and b directions (64.396 Å) and five unit cells tall in the c direction (66.030 Å)]. This was done to improve the long-range Coulomb field over that which was used in the cluster calculations. This new Coulomb field was also broken up into components due to the Cu, O, apical O, and La/Sr sites. These fields were then appropriately scaled based on the orbital occupations from the Hubbard model and the effect was incorporated into the new orbital energies.

As can be seen in Eqs. (1), (2), the self-Coulomb interaction (J_{ii}) is treated separately from the other Coulomb interactions. This is a deviation from the mean-field approximation of Hartree-Fock theory and conventional LDA band-structure calculations. The mean-field approximation would instead use the orbital energy correction equation:

$$E_i = E_i^0 - \sum_j (2 - N_j) \left(J_{ij} - \frac{1}{2} K_{ij} \right). \quad (3)$$

While Eq. (3) may be adequate for many materials, it breaks down in the limit of weakly interacting particles where the self-Coulomb terms are much larger than the coupling matrix elements ($J_{ii} \gg T_{ij}$). As can be seen from the data in Table II, this is the case for $\text{La}_{1.85}\text{Sr}_{0.15}\text{CuO}_4$. In this regime, Eqs. (1), (2) become valid. The difference between Eqs. (1), (2), and (3) can be seen when one orbital is at half occupancy ($N_i = 1$). In Eq. (2) the orbital energy is lowered by the full J_{ii} term while in Eq. (3) the orbital energy is only lowered by ($J_{ii} - \frac{1}{2}K_{ii}$) or equivalently $\frac{1}{2}J_{ii}$. Equations (1), (2) assume that correlation localizes all spins, while Eq. (3) inappropriately assumes the system has ionic character.

Variations on the type of correlation expressed in Eqs. (1), (2) have been introduced by several authors^{4,5} in studies of La_2CuO_4 . However, the self-interaction correction has previously been applied only in a limited fashion to the undoped antiferromagnetic state of the material. Svane,⁴ for example, uses a procedure in which the self-interaction correction is applied only to those orbitals that can be well localized, arguing that the self-Coulomb energy goes to zero for delocalized orbitals. The correction affects only the ener-

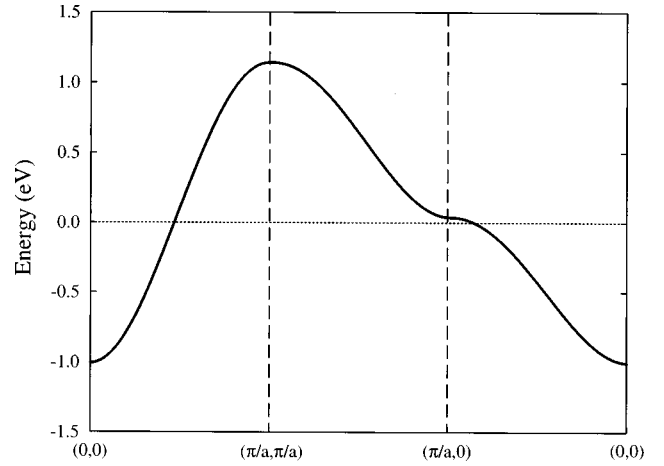


FIG. 2. Dispersion of the top band along symmetry lines when the mean-field equation (3) is used in the Hubbard model. The scaled parameter set of Table III is used and no O p_π to La/Sr charge transfer is included. Other bands are several eV lower in energy and are not shown.

gies of the occupied orbitals, shifting their energies down with respect to the unoccupied orbitals, thus producing a band gap. Without a self-interaction correction, no gap is seen in the undoped system. However, $\text{La}_{2-x}\text{Sr}_x\text{CuO}_4$ is known to be metallic when overdoped. In this phase, orbitals cannot be well localized because the spins are not ordered as in the antiferromagnetic state. Yet it should be argued that local correlation still leads to a self-interaction correction even when the band orbitals are delocalized. Thus, here the self-interaction correction is taken further than before and is applied to *all* orbitals (occupied or unoccupied) by modifying the atomic orbital energies. We have not included spin polarization, so a metallic state is expected with no orbital localization or band gap as in the undoped antiferromagnetic state. As will be seen, the introduction of this correction through Eqs. (1), (2) has the effect of lowering the energy of a partially occupied band with respect to other bands. This is critical to obtaining a Fermi level band crossing in $\text{La}_{1.85}\text{Sr}_{0.15}\text{CuO}_4$.

III. RESULTS

In Figs. 2 and 3, we show the relevant two-dimensional (2D) dispersion for optimally doped $\text{La}_{1.85}\text{Sr}_{0.15}\text{CuO}_4$ as obtained with our Hubbard model using the scaled parameter set of Table III. This doping level corresponds to the removal of a total of 1.15 electrons per unit cell from the Cu/O/apical O bands (undoped La_2CuO_4 has 1 electron per unit cell removed from these bands). As shown in Fig. 2, when our Hubbard model employs the standard mean-field equation (3), the familiar band structure picture is reproduced. A single isolated band having “ B_{1g} ” Cu $d_{x^2-y^2}$ and O p_σ character is seen to cross the Fermi level. The other five bands in this model are buried and not shown here for clarity. The dispersion of the x^2-y^2 band is in excellent agreement with the large scale LDA band structure calculations of Yu *et al.*,¹³ Mattheiss,¹⁴ and others.¹⁵ This agreement should lend validity to our general approach.

As shown in Fig. 3, however, when the self-interaction correction is included in our Hubbard model using Eqs. (1),

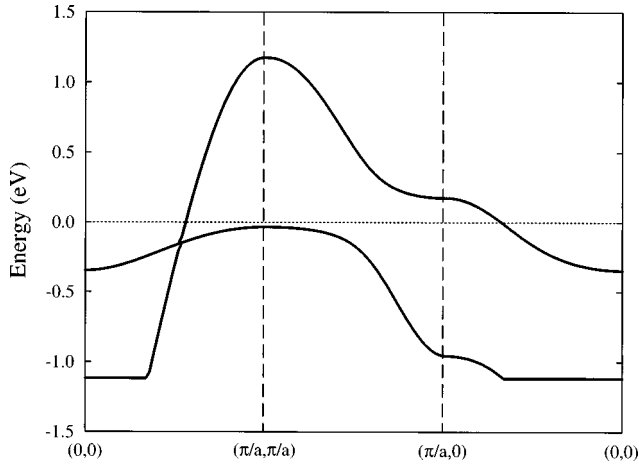


FIG. 3. Dispersion of the top two bands along symmetry lines when the self-interaction corrected Eqs. (1), (2) are used in the Hubbard model. The Fermi level is shown to lie just above the top of the lower band and only 0.153 eV above the crossing point along the $(0,0) - (\pi/a, \pi/a)$ symmetry line.

(2), two bands are seen at the Fermi level. While no holes have been created in the lower band the Fermi level is just 0.035 eV above the top of this band. More importantly, a rigorous crossing, which is critical to the proposed theory, is seen just 0.153 eV below the Fermi level along the $(0,0) - (\pi/a, \pi/a)$ symmetry line [note, there are actually four crossing points in the full 2D Brillouin zone at (k,k) , $(k, -k)$, $(-k,k)$, and $(-k, -k)$]. The close proximity of this crossing to the Fermi level, as determined from this simple model, is a significant finding. Given errors in the Hubbard parameters and missing electronic effects, it is not difficult to conclude that a band crossing, required of the IBP model, indeed appears to occur at the Fermi level of the optimally doped superconductor. This crossing can be characterized as arising between a broad “ B_{1g} ” band dominated by Cu $d_{x^2-y^2}$ character and a narrower “ A_{1g} ” band dominated by Cu d_{z^2} character. The orbital energies and occupations that were computed self-consistently from the model using Eqs. (1), (2) are given in Table IV.

The difference between the conventional band structure and this self-interaction corrected band structure can be seen in Fig. 4. In the conventional band structure [Fig. 4(a)] the top band is dominated by Cu $d_{x^2-y^2}$ character, the two bands at -4 eV are apical O p_x in character, the two bands at -7 eV are O p_σ in character, and the band at -9 eV is dominated by Cu d_{z^2} character. Ligand field theory predicts that

TABLE IV. Computed orbital energies and orbital occupations for optimally doped $\text{La}_{1.85}\text{Sr}_{0.15}\text{CuO}_4$ taken from our Hubbard model using the scaled parameter set of Table III and no O p_π to La/Sr charge transfer. All energies are relative to the Fermi level (in eV).

Orbital	Energy	Occupation
Cu x^2-y^2	-2.570	1.572
Cu z^2	-1.663	1.785
O p_σ	-4.254	1.806
O(2) p_z	-1.611	1.941

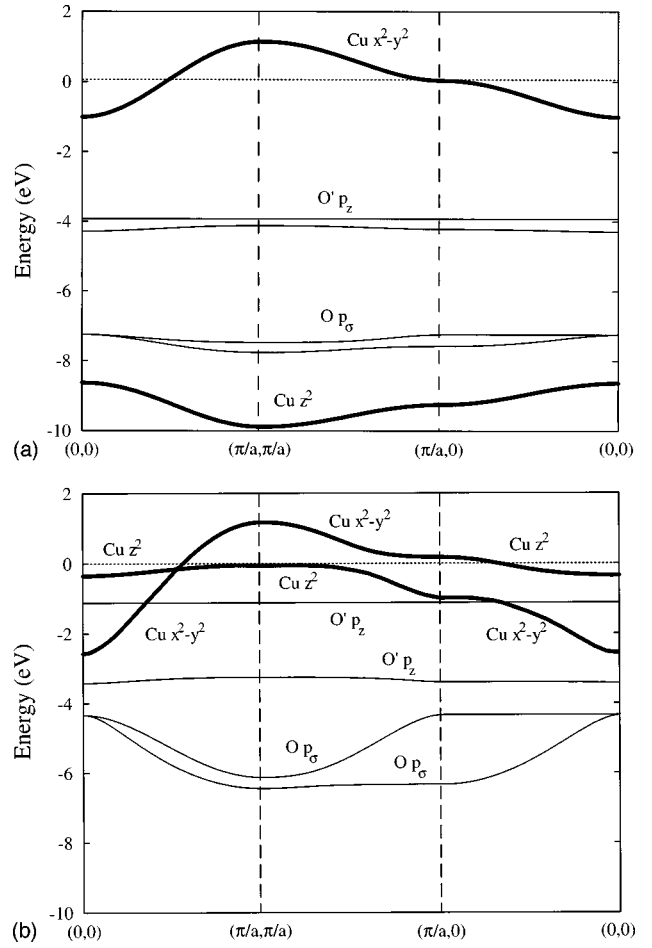


FIG. 4. (a) Complete Hubbard model band structure using the mean-field equation (3). Only the Cu $d_{x^2-y^2}$ band is seen to cross the Fermi level. The Cu d_{z^2} band is at -9 eV. (b) Complete Hubbard model band structure using the self-interaction corrected equations (1), (2). Both the Cu $d_{x^2-y^2}$ and d_{z^2} bands are seen at the Fermi level.

the Cu $d_{x^2-y^2}$ orbital is the most unstable and d_{z^2} is the next most unstable in the Jahn-Teller distorted octahedron of CuO_6 , and the conventional band structure is consistent with this. However, ligand field theory alone cannot explain the 9 eV difference in energy between the two bands generated from these d orbitals. This large energy difference is due to an improper treatment of the self-Coulomb energy. Using the mean-field equation (3), as electrons are removed from the $d_{x^2-y^2}$ orbital, its orbital energy remains artificially high with respect to all other orbitals due to the incorrect accounting of the self-Coulomb energy. As a result, these calculations predict that the $d_{x^2-y^2}$ band is completely emptied upon doping before electrons are removed from another d band. This is chemically unreasonable. When the self-interaction correction is properly included in Eqs. (1), (2), as electrons are removed from the $d_{x^2-y^2}$ orbital, the energy of this orbital is stabilized with respect to the d_{z^2} orbital (and other d orbitals) as a result of reduction in its self-Coulomb energy. At some point then it becomes more favorable to remove electrons from the d_{z^2} orbital. As seen in Fig. 4(b) at optimal doping, the d_{z^2} band is at the Fermi level. Furthermore, it should be noted that as electrons are removed from the d_{z^2} orbital the energy of this orbital stabilizes with re-

spect to the $d_{x^2-y^2}$ orbital. Yet because the self-Coulomb energy of the d_{z^2} orbital is smaller than that of the $d_{x^2-y^2}$ orbital due to $s-d_{z^2}$ hybridization, it is actually possible to remove *more* electrons from the d_{z^2} orbital than the $d_{x^2-y^2}$ orbital. Such considerations are important since they lead directly to the observed band crossing.

To take our calculations one step further, we considered what electronic effects might be missing that would have the greatest effect on the position of the crossing point relative to the Fermi level. Besides errors that might be present in the basic Hubbard parameters due to basis set limitations, cluster size, and the DFT method itself, a number of missing key electronic effects can be identified. All are expected to lead to only minor perturbations of the band structure, but their cumulative effect could have an impact on the position of the band crossing. These effects include:

- (1) Explicit inclusion of z -axis dispersion instead of the perturbative approach taken here.
- (2) Inclusion of additional Hubbard parameters. Additional parameters should all be <0.04 eV.
- (3) Explicit inclusion of other bands. Small mixings with other bands, in particular the $\text{Cu}d_{xy}/\text{O}p_{\pi}$ band, could have an effect on the position of the crossing.
- (4) Use of more realistic charges in the cluster calculations.
- (5) Inclusion of additional spin correlation. The current model only includes the self-interaction correction to account for the tendency of weakly interacting systems to localize spin. However, spin couplings between different orbitals, in particular the triplet coupling between $\text{Cu}d_{x^2-y^2}$, and d_{z^2} , has been ignored.
- (6) Explicit inclusion of the La and Sr ions. The current model treats these atoms as single point charges having the appropriate average of the formal charges $+3.0$ for La and $+2.0$ for Sr. In reality, these ions are likely less highly charged and have spatial extent which leads to Pauli repulsions. Treatment of the two ions as distinct should lead to local perturbations of Hubbard parameters.
- (7) Inclusion of the orthorhombic distortion. The crystal in the superconducting phase is distorted from its high-symmetry tetragonal (D_{4h}) structure to a lower symmetry orthorhombic (C_{2h}) structure.¹¹ This is manifested by a tilting of the CuO_6 units or equivalently a buckling of the CuO_2 planes. An important effect from this distortion is that two of the four crossing points [at $(k, -k)$ and $(-k, k)$] become strictly avoided due to the reduced symmetry. However, it should be stressed that the other two crossing points [at (k, k) and $(-k, -k)$] are maintained, which is critical to the proposed IBP theory.

While it is not clear that all of these effects are favorable in terms of moving the band crossing toward the Fermi level, their combined effect could easily lead to such a change. We stress that a perturbation of only 0.153 eV (a small quantity on the chemical scale) is necessary to observe a Fermi level crossing.

We have, in fact, applied a specific perturbation to our model in order to incorporate one of the above effects. Investigations of the effect of La and Sr using a variety of

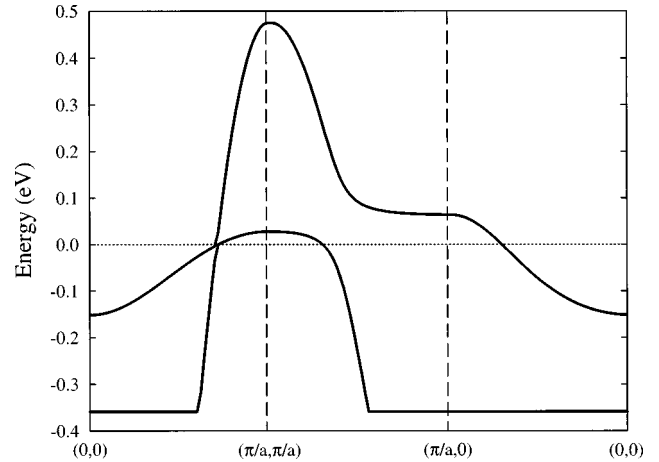


FIG. 5. Dispersion of the top two bands along symmetry lines when a 0.50 electron $\text{O} p_{\pi}$ to La/Sr charge transfer is included in the self-interaction corrected Hubbard model. The Fermi level is shown to coincide with the crossing point along the $(0,0) - (\pi/a, \pi/a)$ symmetry line.

clusters at the BLYP level showed significant mixing of the $\text{O} p_{\pi}$ orbitals with the orbitals of these metals. The implication of these results is that there is diffusion of the $\text{O} p_{\pi}$ electrons onto the La/Sr sites which has been ignored by the CuO_6 cluster calculations. The effect of this charge diffusion is to lower the energy of both the $\text{O} p_{\sigma}$ and $\text{O} p_{\pi}$ orbitals and raise the energy of the apical $\text{O} p_z$ orbitals relative to the Cu orbitals. To account for this effect we included in our Hubbard model calculations an adjustable parameter which defined the extent of charge transfer from $\text{O} p_{\pi}$ to La/Sr. While we do not explicitly include these π bands in the final model, Coulomb terms for the $\text{O} p_{\pi}$ orbitals were evaluated and included in Tables II and III (La and Sr were still treated as classical point charges). This allowed us to include the effect of charge transfer by altering the Coulomb field in a fashion similar to that explained in Sec. II B. Orbital energies were reevaluated to reflect the change in the Coulomb field due to this charge transfer.

The primary effect of this charge transfer is to stabilize the π bands relative to the Fermi level by significantly lowering the orbital energy of $\text{O} p_{\pi}$. A secondary effect, however, is to raise the crossing point of the two bands of interest closer to the Fermi level for the optimally doped system. This was accomplished when the charge-transfer term was empirically adjusted to the value of 0.50 electrons transferred. That is, the charge on the La/Sr sites was $+2.425$ compared to the formal charge of $+2.925$. This should be considered within the range of reasonable charges for these ions (note the charges on the other atoms are $+1.563$ for Cu, -1.429 for O, and -1.777 for apical O). We should note though, that the extent of charge transfer calculated here may be an overestimate in light of the fact that the other electronic effects listed above have not yet been incorporated. But, as detailed in the accompanying article by Tahir-Kheli,⁶ the resulting band structure proves to have the necessary features to explain a number of key experiments.

The 2D dispersion of the top two bands from these calculations is shown in Fig. 5 and the optimized orbital energies and occupations are given in Table V. In addition the Fermi

TABLE V. Computed orbital energies and orbital occupations for optimally doped $\text{La}_{1.85}\text{Sr}_{0.15}\text{CuO}_4$ taken from our Hubbard model using the scaled parameter set of Table III and 0.50 electron $\text{O } p_\pi$ to La/Sr charge transfer. All energies are relative to the Fermi level (in eV).

Orbital	Energy	Occupation
$\text{Cu } x^2-y^2$	-2.403	1.770
$\text{Cu } z^2$	-2.092	1.666
$\text{O } p_\sigma$	-6.122	1.929
$\text{O}(2) p_z$	-0.852	1.777

surfaces are shown in Fig. 6 and the density of states of the top two bands is shown in Fig. 7.

IV. DISCUSSION

A. Band structure of $\text{La}_{1.85}\text{Sr}_{0.15}\text{CuO}_4$

The band crossing we observe arises from the following considerations. In this discussion, we will refer to the two bands that cross as the “ B_{1g} ” and “ A_{1g} ” bands. The crossing produces two new bands that touch, referred to as U (pper) and L (ower). The dispersion of the B_{1g} band, dominated by $\text{Cu } d_{x^2-y^2}$ character, is rather broad, on the order of 2 eV, producing a low density of states. The dispersion of the A_{1g} band, dominated by $\text{Cu } d_{z^2}$ character, is in contrast rather narrow, on the order of 0.3 eV, producing a high density of states. At the $(\pi/a, \pi/a)$ point, the higher energy band is B_{1g} in nature, corresponding to the completely antibonding combination of $\text{Cu } d_{x^2-y^2}$ and $\text{O } p_\sigma$ orbitals. The lower energy band is A_{1g} in nature, corresponding to the antibonding combination of the $\text{Cu } d_{z^2}$, $\text{O } p_\sigma$, and apical $\text{O } p_z$ orbitals. At the $(0,0)$ point, however, the higher energy band is A_{1g} in nature and the lower energy band is B_{1g} . Due to this change in the relative energetics between the top of both bands and the bottom of both bands, the B_{1g} and A_{1g} bands must cross, producing a U band and L band which each have both B_{1g} and A_{1g} character. This crossing of bands is strictly avoided everywhere except for one point in the 2D Brillouin zone. Along the $(0,0) - (\pi/a, \pi/a)$ symmetry line, the crossing is rigorously allowed since the B_{1g} and A_{1g} orbitals cannot mix

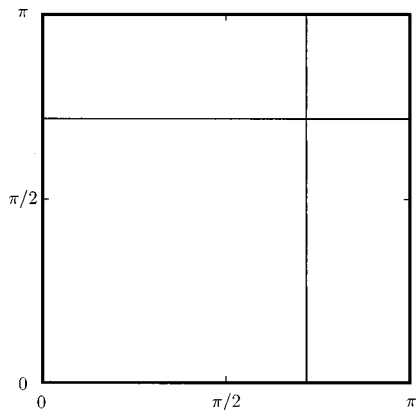


FIG. 6. Fermi surface showing the touching of the upper and lower bands along the $(0,0) - (\pi/a, \pi/a)$ symmetry line. The squareness of this surface is expected to change with the addition of longer range terms.

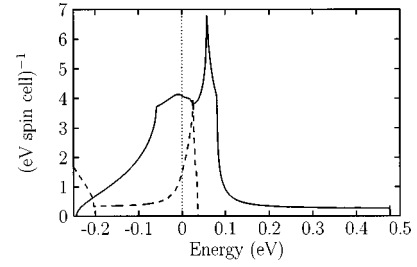


FIG. 7. Density of states of the top two bands shown from $E = -0.25$ to $+0.50$ eV.

along this direction. Due to this rigorous crossing, the U band and L band must touch. While the position of this crossing point (or touching point) is subject to variation, its existence is quite robust over a wide range of model parameters.

In the closeup of the density of states shown in Fig. 7, it can be seen how the crossing of the B_{1g} and A_{1g} bands affects the nature of the U and L bands. The U band starts at $+0.47$ eV and represents the $(\pi/a, \pi/a)$ point of the B_{1g} band. The density of states of this band remains consistently low until about $+0.10$ eV where there is a sharp peak. This peak represents the change in character of the band from B_{1g} to A_{1g} in the vicinity of the $(\pi/a, 0)$ point. The density of states of the U band remains relatively high at energies below this point, being dominated by A_{1g} character. The band terminates at -0.25 eV, which represents the $(0,0)$ point of the A_{1g} band. The onset of the L band is characterized by a sharp peak in the density of states at $+0.03$ eV. This peak occurs in the vicinity of the $(\pi/a, \pi/a)$ point of the A_{1g} band. The peak comes down to a low density of states near the Fermi level and the density of states remains low, being dominated by B_{1g} character until about -0.20 eV when character from other orbitals (in particular the A_{2u} antibonding combination of the apical $\text{O } p_z$ orbitals) starts to mix in. The change in character of this band at lower energies should have no effect on the issue of the band crossing or the IBP model.

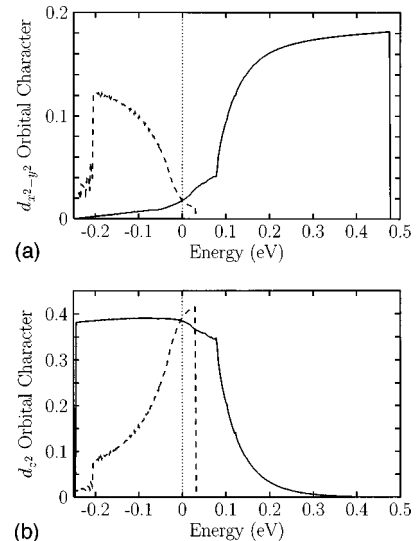


FIG. 8. (a) Extent of $\text{Cu } d_{x^2-y^2}$ orbital character in the upper (solid line) and lower (dashed line) bands. (b) Extent of $\text{Cu } d_{z^2}$ orbital character.

The character of these bands can be seen more clearly in Fig. 8. In Fig. 8(a) the U band is shown to be dominated by Cu $d_{x^2-y^2}$ character above 0.10 eV, while the L band is dominated by $d_{x^2-y^2}$ below the Fermi level. In Fig. 8(b), the U band is shown to be dominated by Cu d_{z^2} character below 0.10 eV while the L band is dominated by d_{z^2} only at the Fermi level.

While most band-structure calculations have only shown a single band at the Fermi level,¹⁵ we argue that this is due to the lack of a proper accounting of the self-Coulomb energy. We should note however, Shiraishi *et al.*¹⁶ who included the effect of spin polarization, found that doping of La_2CuO_4 resulted in the formation of two types of holes from two distinct bands. While no band crossing was noted, the two types of holes were characterized as being Cu $d_{x^2-y^2}$ and d_{z^2} . Eto, Saito, and Kamimura¹⁷ also suggested the importance of the Cu d_{z^2} orbital based on cluster model calculations. We find that this work lends support to the findings reported here.

B. Band structure of related materials

Certain qualitative features in the density of states for $\text{La}_{2-x}\text{Sr}_x\text{CuO}_4$ (LASCO) should be characteristic of many superconducting copper oxide materials, such as $\text{YBa}_2\text{Cu}_3\text{O}_{6+\delta}$ (YBCO), $\text{Bi}_2\text{Sr}_2\text{Ca}_{n-1}\text{Cu}_n\text{O}_{2n+6+\gamma}$, $\text{Tl}_2\text{Ba}_2\text{Ca}_{n-1}\text{Cu}_n\text{O}_{2n+4+\delta}$, and others. Each should be characterized by a peak in the U band just above the top of the L band. This is due to band repulsions away from the $(0,0) - (\pi/a, \pi/a)$ diagonal which introduce A_{1g} character into the U band. When these band repulsions are large enough [such as they are at $(\pi/a, 0)$], the peak in the density of states of the U band should occur above the top of the L band. The L band, on the other hand, should have a sharp peak at its onset at $(\pi/a, \pi/a)$ which vanishes as the band becomes B_{1g} in character.

Although the electronic structure of YBCO (Fig. 9) should share common features with LASCO, it differs in one important regard: the local symmetry of YBCO in the superconducting state is D_{2h} as compared to C_{2h} for LASCO.¹¹ This symmetry will not allow a rigorous crossing of the two bands along the diagonal (or any other point) in the 2D Brillouin zone. However, it should be recognized that the dual CuO_2 planes of YBCO lead to four bands in contrast to the two bands of LASCO. Dispersion of these four bands in the z direction leads to two bands having A_g symmetry at $k_z = 0$ and $k_z = \pi/c$ and two bands having B_{1u} symmetry. The two A_g bands are principally composed of the bonding combinations of the Cu $d_{x^2-y^2}$ orbitals from the two planes and the bonding combinations of the Cu d_{z^2} orbitals from the two planes. The B_{1u} bands are the antibonding analogues. While the two A_g bands are not precluded from mixing at any symmetry point, and the two B_{1u} bands are also not precluded from mixing, the A_g and B_{1u} bands cannot mix when $k_z = 0$ or $k_z = \pi/c$. This suggests that crossings could occur between the A_g bands and the B_{1u} bands. Based on this idea, we propose the following scenario. (Note, we do not address the effects of the chain CuO bands, but we suspect the essential topology described below holds.)

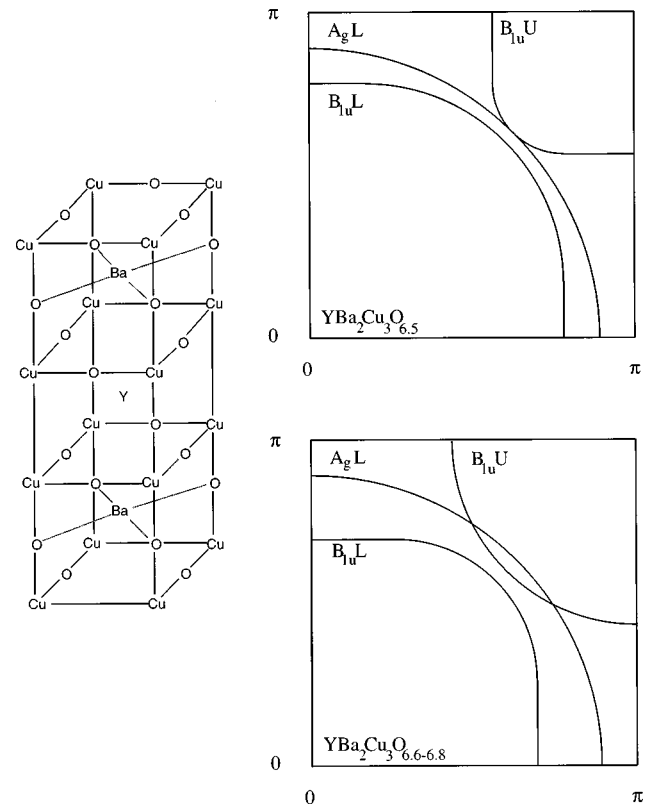


FIG. 9. Schematic depiction of Fermi surfaces for $\text{YBa}_2\text{Cu}_3\text{O}_{6+\delta}$. The onset of superconductivity is expected when the $B_{1u} U$ band and the $A_g L$ band first cross at $k_z = \pi/c$ (top). Superconductivity continues upon further doping (bottom). A change in T_c may be expected when a similar set of crossings appears for $k_z = 0$. The YBCO unit cell is shown (left).

There are two sets of two bands (U and L) having qualities similar to those shown here for LASCO. One set has A_g symmetry while the other has B_{1u} symmetry. The primary difference between these bands and those of LASCO is that the crossing along the $(0,0) - (\pi/a, \pi/a)$ direction is avoided. Since the Cu $d_{x^2-y^2}$ dispersion in the z direction is expected to be small, the $d_{x^2-y^2}$ components of these bands (analogous to the B_{1u} bands of LASCO) should be nearly degenerate. In contrast, the Cu d_{z^2} components of these bands (analogous to the A_{1g} bands of LASCO) should be separated in energy.

The onset of superconductivity in YBCO should occur when the Fermi level coincides with a band crossing. This likely occurs at $k_z = \pi/c$ between the $B_{1u} U$ band (which is completely antibonding in the z direction) and the $A_g L$ band. Interestingly, it is not required to occur along the $(0,0) - (\pi/a, \pi/a)$ direction. In fact, there is likely a double crossing within a quadrant of the Brillouin zone, as depicted in Fig. 8. In this schematic, we view the Fermi surfaces as squared circles centered around $(0,0)$ for $B_{1u} L$ and $A_g L$ and centered around $(\pi/a, \pi/a)$ for $B_{1u} U$. Superconductivity begins when the $A_g L$ and $B_{1u} U$ bands first touch. Since the radius of the $B_{1u} U$ Fermi surface is increasing faster than the radius of the $A_g L$ Fermi surface is decreasing (due to the difference in their densities of states), two crossing points can be sustained over a wide doping range. At sufficiently higher doping levels, a second set of band crossings of a

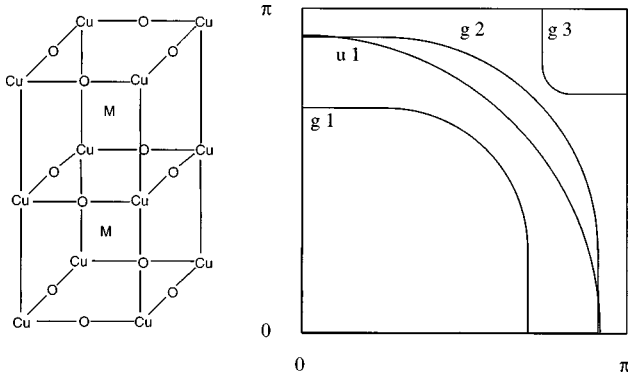


FIG. 10. Schematic depiction of Fermi surfaces for a typical three-plane copper oxide superconductor. Band repulsions may lead to highly coincident $g2$ and $u1$ surfaces in the vicinity of $(\pi/a, 0)$ when $k_z=0$ or $k_z=\pi/c$.

similar nature should occur at $k_z=0$. This proposal easily explains the extended doping range observed for YBCO and the appearance of two T_c 's in different doping regimes for this material. Furthermore, it suggests a reason for the increasing T_c for LASCO vs underdoped YBCO vs optimally doped YBCO. We correlate an increase in the number of crossing points, or, more correctly, the number of crossing points which are thermally accessible, to an increase in T_c . Indeed, it is observed that superconductivity begins with $\text{YBa}_2\text{Cu}_3\text{O}_{6.6}$ showing a T_c of 60 K. This T_c is sustained upon further doping until a rapid increase to $T_c=90$ K is observed near $\text{YBa}_2\text{Cu}_3\text{O}_{6.9}$. Further doping to $\text{YBa}_2\text{Cu}_3\text{O}_{7.0}$ maintains T_c at this higher temperature.¹⁸

Similar analysis can be applied to the bismuth¹⁹ and thallium²⁰ systems. We note that in these systems an increase in T_c is correlated with an increase in the number of CuO_2 planes per unit cell. Following the above arguments this makes sense in that it leads to more bands which produce more band crossings as shown schematically in Fig. 10. For a three-plane system we are now dealing with six bands. Four of these bands will be symmetric with respect to reflection through the middle plane (bands $g1$, $g2$, $g3$, and $g4$) and two of these bands will be antisymmetric (bands $u1$ and $u2$). We argue that band repulsions near the $(\pi/a, 0)$ point, as seen in the LASCO band structure, would be stronger for the g bands, since d_{z^2} character should appear in these bands at a higher energy than in the u bands. This could produce a crossing between the $u1$ and $g2$ bands at $k_z=0$ and $k_z=\pi/c$ as depicted in the figure. Since the two surfaces might be expected to be highly coincident at this point, the number of thermally accessible crossing points should be high. Clearly, it can be seen that the addition of more CuO_2 planes

increases the probability of favorable crossing situations as illustrated here, and this should lead to potentially higher T_c 's.

Finally we wish to note that $\text{Nd}_{2-x}\text{Ce}_x\text{CuO}_4$ (Ref. 21) is electron doped in contrast to the majority of copper oxide superconductors which are hole doped. This may suggest that the "undoped" system is actually overdoped. Alternatively, it may suggest that the nature of the two bands that cross is substantially different. While we anticipate that one of the bands will be B_{1g} Cu $d_{x^2-y^2}$ in character, the other band may not be A_{1g} Cu d_{z^2} since this band is expected to appear only as electrons are removed from the system. We suggest instead that the second band is a Nd/Ce band. It follows from this suggestion that high-temperature superconductivity is not dependent on the specific crossing of the Cu $d_{x^2-y^2}$ and d_{z^2} bands. We stress, in fact, the only requirement of the IBP model that we now see is that some sort of crossing of bands occurs at the Fermi level. This leads us to be optimistic that with the careful exploitation of symmetry, entirely new classes of high-temperature superconductors will be developed in our future.

V. CONCLUSION

We have presented the results of a Hubbard model calculation on the optimally doped superconducting material $\text{La}_{1.85}\text{Sr}_{0.15}\text{CuO}_4$. We conclude from these calculations that there is a crossing of two bands which occurs at the Fermi level. One of these bands is B_{1g} in character, dominated by Cu $d_{x^2-y^2}$ and the other is A_{1g} in character, dominated by Cu d_{z^2} . The crossing rigorously occurs along the $(0, 0) - (\pi/a, \pi/a)$ symmetry line of the 2D Brillouin zone. As detailed in the preceding paper by Tahir-Kheli,⁶ an interband pairing (IBP) of electrons between these two bands leads to superconductivity. It can only occur at the critical doping level where the Fermi energy coincides with the band crossing, i.e., $x=0.15$. The resulting density of states from this work is used in the accompanying work to explain a number of key experiments on this material.

Extension of the band model obtained for LASCO in these calculations to YBCO provides an easy explanation for the observation of a wide doping range for superconductivity to occur in this material as well as an explanation for the observation of two T_c 's in different doping regimes. We anticipate at this point that other materials will be similarly understood largely through geometric considerations.

ACKNOWLEDGMENT

The authors wish to thank Dr. Jean-Marc Langlois for many useful discussions.

¹J. G. Bednorz and K. A. Müller, Z. Phys. B **64**, 189 (1986).

²J. Tahir-Kheli, in *Proceedings of the 10th Anniversary HTS Workshop on Physics, Materials and Applications*, edited by B. Batlogg, C. W. Chu, W. K. Chu, D. U. Gubser, and K. A. Müller (World Scientific, River Edge, NJ, 1996), pp. 491–492.

³H. Takagi, R. J. Cava, M. Marezio, B. Batlogg, J. J. Krajewski,

W. F. Peck, Jr., P. Bordet, and D. E. Cox, Phys. Rev. Lett. **68**, 3777 (1992).

⁴A. Svane, Phys. Rev. Lett. **68**, 1900 (1992).

⁵V. I. Anisimov, F. Aryasetiawan, and A. I. Lichtenstein, J. Phys.: Condens. Matter **9**, 767 (1997).

⁶J. Tahir-Kheli, preceding paper, Phys. Rev. B **58**, 12 307 (1998).

- ⁷J. C. Slater, *Quantum Theory of Molecules and Solids, Vol. 4: The Self-Consistent Field for Molecules and Solids* (McGraw-Hill, New York, 1974); A. D. Becke, Phys. Rev. A **38**, 3098 (1988); C. Lee, W. Yang, and R. G. Parr, Phys. Rev. B **37**, 785 (1988); implemented as described in B. Miehlich, A. Savin, H. Stoll, and H. Preuss, Chem. Phys. Lett. **157**, 200 (1989).
- ⁸W. J. Hehre and J. A. Pople, J. Chem. Phys. **56**, 4233 (1972).
- ⁹P. J. Hay and W. R. Wadt, J. Chem. Phys. **82**, 299 (1985).
- ¹⁰M. N. Ringnalda, J.-M. Langlois, R. B. Murphy, B. H. Greeley, C. Cortis, T. V. Russo, B. Marten, R. E. Donnelly, Jr., W. T. Pollard, Y. Cao, R. P. Muller, D. T. Mainz, J. R. Wright, G. H. Miller, W. A. Goddard III, and R. A. Friesner, JAGUAR (formerly PS-GVB) v2.3, Schrödinger, Inc., 1996.
- ¹¹R. M. Hazen, in *Physical Properties of High Temperature Superconductors II*, edited by D. M. Ginsberg (World Scientific, New Jersey, 1990), 121–198.
- ¹²J. Pipek and P. G. Mezey, J. Chem. Phys. **90**, 4916 (1989).
- ¹³J. Yu, A. J. Freeman, and J. H. Xu, Phys. Rev. Lett. **58**, 1035 (1987).
- ¹⁴L. F. Mattheiss, Phys. Rev. Lett. **58**, 1028 (1987).
- ¹⁵W. E. Pickett, Rev. Mod. Phys. **61**, 433 (1989), and references therein.
- ¹⁶K. Shiraiishi, A. Oshiyama, N. Shima, T. Nakayama, and H. Kamimura, Solid State Commun. **66**, 629 (1988).
- ¹⁷M. Eto, R. Saito, and H. Kamimura, Solid State Commun. **71**, 425 (1989).
- ¹⁸R. J. Cava, B. Batlogg, C. H. Chen, E. A. Rietman, S. M. Zahurak, and D. Werder, Nature (London) **329**, 423 (1987).
- ¹⁹C. Michel, M. Hervieu, M. M. Borel, A. Grandin, F. Deslandes, J. Provost, and B. Raveau, Z. Phys. B **68**, 421 (1987); H. Maeda, Y. Tanaka, M. Fukutomi, and T. Asano, Jpn. J. Appl. Phys., Part 2 **27**, L209 (1988).
- ²⁰Z. Z. Sheng and A. M. Hermann, Nature (London) **332**, 55 (1988); **332**, 138 (1988).
- ²¹Y. Tokura, H. Takagi, and S. Uchida, Nature (London) **337**, 345 (1989).